Journal of Materials Chemistry C

Directed Polymorphism and Mechanofluorochromism of Conjugated Materials through Weak Non-Covalent Control

Journal:	*Journal of Materials Chemistry C*
Manuscript ID	TC-ART-03-2019-001301.R1
Article Type:	Paper
Date Submitted by the Author:	20-May-2019
Complete List of Authors:	Sharber, Seth; Tufts University, Chemistry Mann, Arielle; Tufts University, Chemistry Shih, Kuo-Chih; University of Connecticut System, Department of Chemical and Biological Engineering Mullin, William; Tufts University, Chemistry Nieh, Mu-Ping; University of Connecticut, Chemical and Biomolecular Engineering; University of Connecticut, Polymer Program, Institute of Materials Science Thomas, Samuel; Tufts University, Chemistry

SCHOLARONE™
Manuscripts

Journal Name

ARTICLE

Directed Polymorphism and Mechanofluorochromism of Conjugated Materials through Weak Non-Covalent Control

Seth A. Sharber[a], Arielle Mann[a], Kuo-Chih Shih[b], William J. Mullin, Mu-Ping Nieh[b], Samuel W. Thomas III[a]*

Received 00th January 20xx,
Accepted 00th January 20xx

DOI: 10.1039/x0xx00000x

www.rsc.org/

Understanding and manipulating crystal polymorphism can provide novel strategies for materials discovery in organic optoelectronics. In this paper, a series of seven ester-terminated three-ring phenylene ethynylenes (PEs) exhibit structure-dependent polymorphism wherein alkyl chain length modulates the propensity to form violet or green fluorescent solid phases, as well as tunable thermal and mechanofluorochromic (MFC) transitions. These compounds harness "soft" non-covalent control to achieve polymorphism: the electronic substituent effect of the ester groups weakens the fluoroarene-arene (ArF-ArH) interactions that typically direct crystal packing of this class of compounds, increasing competitiveness of other interactions. Small structural modifications tip this balance and shift the prevalence of violet- or green-emitting polymorphs. Compounds with short alkyl chain lengths show both violet and various green fluorescent polymorphs, while the violet fluorescent form dominates with alkyl lengths longer than butyl. Further, thermally induced green-to-violet fluorescent crystal-to-crystal transitions occur for single crystals of **CO2-1** and **CO2-3**. Finally, the PEs show reversible violet-to-green mechanofluorochromism (MFC), with temperature required for reversion of this MFC decreasing with alkyl chain length. We therefore present this design of directional but weak interactions as a strategy to access polymorphs and tunable stimuli-responsive behavior in solids.

Introduction

The challenge of predicting conformation and molecular assembly in the solid state makes the bottom-up design of functional organic materials difficult.[1–3] This goal is particularly elusive in the design of responsive materials, which hold promise for numerous applications by exhibiting phenomena such as mechanofluorochromic (MFC), photochromic, thermochromic, and vapochromic materials.[4–6] Since access to solid phases with different optoelectronic properties is important in many such designs, crystal polymorphs can provide important structural insights in the distinct properties of interconvertible phases. Molecules that present numerous directional interactions of similar energies can form responsive materials that switch between packing motifs with different photophysical properties.[5,7–11] Although important advances in the theoretical prediction of polymorphs[12] have emerged, their complex energetic landscapes make rational design of polymorphs and reversibly-responsive solids uniquely challenging, requiring extensive experimental effort to identify, isolate, and characterize polymoprhs.[10,13–16] Therefore, strategies that enable predictable access to polymorphism and control over phase behavior can inform design and discovery of new responsive materials.[17–22]

Some common structural themes exist among compounds that switch between polymorphs in response to stimuli, such as conformational flexibility or torsionally distorted structures that pack inefficiently, for example in the aggregation-induced emission (AIE) luminogens.[4,5,23–28] In addition, supramolecular strategies using directional interactions—synthons such as hydrogen bonding, halogen bonding, and fluoroarene-arene (ArF-ArH) interactions—can direct packing and yield predictable assembly motifs through development of structure-property relationships.[7,20,29–32] Furthermore, polymorphs can emerge when the energetics of competing directional interactions are judiciously balanced, as in cases of synthon polymorphism.[27,29,33,34] As an example, Zou and You reported diaryltriazolo-pyrimidines in which different regioisomeric aryl linkages alter stacking interactions predictably and determine whether bathochromic or hypsochromic MFC behavior occurs.[35] Other design strategies for responsive materials, often based on AIEgens, include setting up competitions between hydrogen bonding and aromatic stacking interactions to yield interconvertible phases with different optical properties.[36–39] Therefore, purposeful integration of competition between directional interactions, especially those with readily tunable strengths, can form the basis for rational design of stimuli-responsive transitions between polymorphs.

[a] *Department of Chemistry, Tufts University, 62 Talbot Avenue, Medford, MA 02155, USA. E-mail: sam.thomas@tufts.edu*
[b] *Department of Chemical & Biomolecular Engineering, University of Connecticut, 97 North Eagleville Road, Storrs, CT 06269, USA*

†Electronic supplementary information (ESI) available: Experimental methods, synthetic methods, NMR spectra, HRMS, photophysical data, DSC data, PXRD data, crystallographic tables. CCDC 1897095 - 1897099

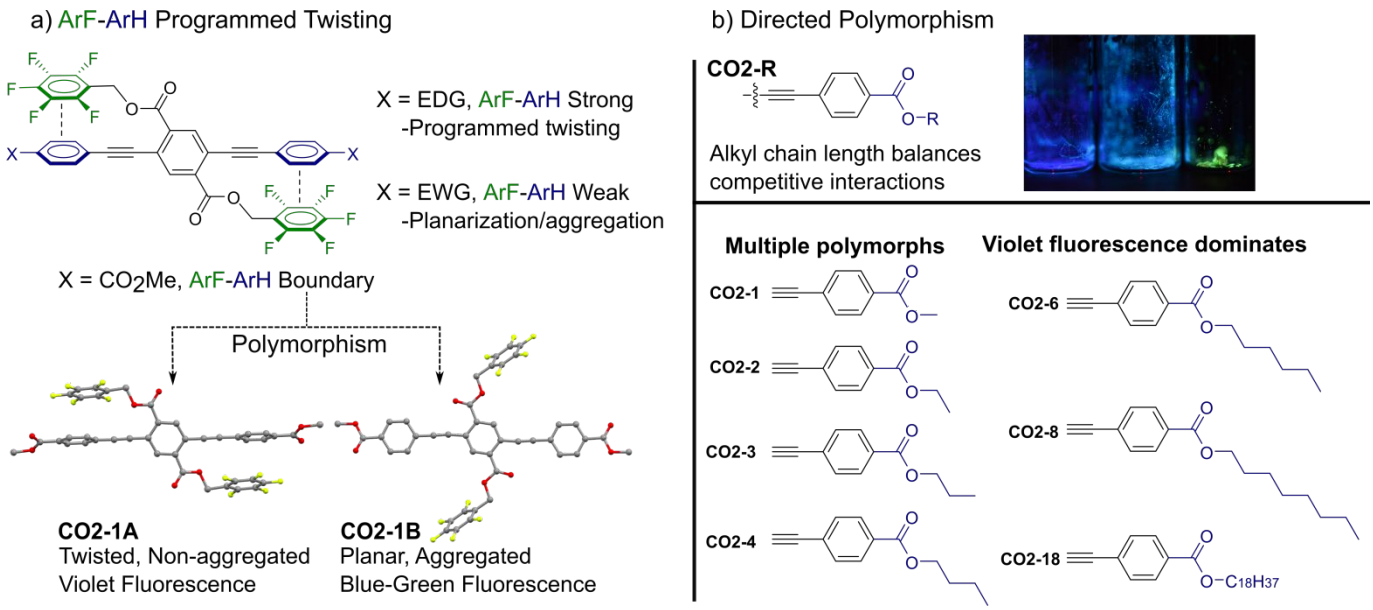

Figure 1. Weak non-covalent control in ester-terminated PEs. a) Substituents in PE main chain affect the ArF-ArH stacking interaction that twists the backbone. When X = CO_2Me, aromatic stacking interactions between PEs become competitive with ArF-ArH programmed twisting, resulting in polymorphism. b) Lengths of alkyl chains alter polymorphism in ester-terminated PEs by tipping the balance of competing interactions; short chain lengths result in multiple polymorphs, while long chain lengths favor the violet fluorescent phase.

Although discovery of MFC materials is often empirical, explicit consideration of the properties of polymorphs can yield structural and mechanistic insight to their behavior.[9,40–44] Among known MFC materials, electronic substituent effects and positional isomerism affect both electronics of conjugated units and crystal packing, enabling dramatic tuning of optical contrast, mechanical sensitivity, and thermal response.[41,45–49] In contrast, although alkyl pendants typically only modulate crystal packing, their lengths can tune MFC shifts, sensitivity to mechanical force, and thermal recovery temperature due to alterations in packing and variation of relative stability of phases.[40,50–56]

Our group has reported tunable MFC properties of three-ring PEs that harness directional, discrete interactions of pendant arenes to program PE conformation and assembly, and thereby control luminescence of these solids.[57-59] Fluoroarene-arene (ArF-ArH) interactions between non-conjugated side chains and PE main chains yield twisted backbones that stack in electronically isolated assemblies, resulting in hypsochromically shifted optical spectra and reversible MFC behavior.[57,58] We further found that electron-donating substituents on the non-fluorinated ring favor these cofacial ArF-ArH interactions and the resulting twisted geometries, while electron-withdrawing groups can weaken the ArF-ArH interactions such that other packing motifs with bathochromically shifted fluorescence emerge.[58] In addition, we also demonstrated alkyl chain length-dependent MFC properties of a series of aniline-terminated derivatives of this common PE scaffold—increasing the lengths of N-terminal alkyl chains lowered the temperatures required for thermal recovery after grinding.[59]

We present here a series of electron-withdrawing ester-terminated three-ring PE analogs that share identical perfluorinated aromatic side chains and differ only in the length of terminal benzoate alkyl chains. In contrast with the strong ArF-ArH interactions of the aniline-terminated PEs, these compounds with ArF-ArH interactions weakened by the electron-withdrawing nature of the ester substituents display prevalent polymorphism. The lengths of the alkyl chains influence both thermally induced crystal-to-crystal transitions and MFC properties of these compounds. Evidence from fluorescence, crystallography, X-ray scattering, and thermal properties of polymorphs reveals that balancing the competitions between non-covalent interactions can enable polymorphism as well as new responsive behavior.

Results and Discussion

1. Design and Synthesis of Target Compounds

Our previous work shows that ArF-ArH cofacial stacking interactions between ArF side chains and ArH rings in PE main chains twist the conjugated arenes out of coplanarity, reducing both intramolecular and intermolecular electronic coupling and hypsochromically shifting luminescence relative to other structures.[57–59] In agreement with previous studies that showed a correlation between Hammett parameters and aromatic interaction strength, we found electronic substituent effects on the ArH ring can dictate whether these solids exhibit these ArF-ArH interactions.[60,58] In this particular series of PEs, methyl ester substituents represented a boundary of whether

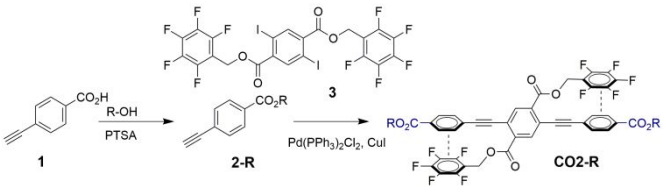

Scheme 1. Synthesis of ester-terminated PEs with varying alkyl chain lengths.

This journal is © The Royal Society of Chemistry 20xx

Please do not adjust margins

ArF-ArH interactions occurred or not. We previously determined crystal structures of two polymorphs, one of which had twisted PEs due to ArF-ArH interactions, while the other had coplanar PEs that aggregated, and no ArF-ArH interactions (Figure 1).

We suspected that small changes in alkyl chain length could influence the apparently delicate balance between these two polymorphs, and therefore prepared a series of analogs of this compound, with varying ester alkoxy chain lengths. Scheme 1 shows the synthesis of these compounds, which followed reported methods:[61] ethynylation of methyl 4-iodobenzoate with trimethylsilyl acetylene followed by simultaneous deprotection of ester and alkyne gave 4-ethynylbenzoic acid (**1**). Esterification of this common intermediate with *n*-alkyl alcohols yielded **2-R,** Sonogashira coupling of which with 2,5-diiodoterephthalate **3** afforded target compounds **CO2-R** with alkyl groups ranging from ethyl to *n*-octadecyl.[59]

2. Properties of PEs in Solution and Thin Films

All molecules in the **CO2-R** series show nearly identical optical properties in solution because differences in alkyl chain lengths do not alter the conjugated π-system directly (Figure 2). Dilute samples of all **CO2-R** samples in chloroform appear colorless with violet emission (Figure 2). Small bathochromic shifts of up to 4 nm occur with increasing chain length (absorbance λ_{max} = 363 – 367 nm, emission λ_{max} = 415 – 419 nm), while fluorescence quantum yields (~0.45) and lifetimes (~1.0 ns) do not depend on alkyl chain length. In addition, optical properties of these compounds depend only slightly on solvent polarity: the emission λ_{max} for **CO2-1** ranges from 417 nm in DMF to 409 nm in hexane with no discernable trend, while quantum yields decrease slightly in higher polarity solvents (0.53 in hexane to 0.36 in DMF, Figure S1 and Table S1).

In contrast, drop-cast films of this series of compounds show some differences in photophysical spectra but no clear trend based on alkyl chain length, all of which exhibit violet fluorescence after slow evaporation under a watch glass and heating to 100-130 °C to drive packing towards the most stable phases.[58] In all cases, colorless and uniform violet emission after annealing showed relatively similar or hypsochromically shifted absorbance and emission spectra relative to chloroform solutions. These films have absorbance λ_{max} of 342 – 355 nm and emission λ_{max} from 385 – 414 nm, representing hypsochromic shifts of 10-20 nm when compared to those in chloroform solution. In contrast, the thermal and mechanical properties of these solids vary regularly with chain length (Table 1): melting points decrease with increasing chain length (214 °C for **CO2-1** to 110 °C for **CO2-18**). In addition, solids with longer alkyl pendants (up until octyl) are increasingly soft, and qualitatively more mechanically compliant, suggesting an overall decrease in crystallinity. Compound **CO2-18** breaks this trend, and noticeably more crystalline and brittle, qualitatively, than **CO2-6** and **CO2-8**. We speculate that dispersion interactions between the long octadecyl chains of **CO2**-18 become increasingly important in this solid, increasing its rigidity.

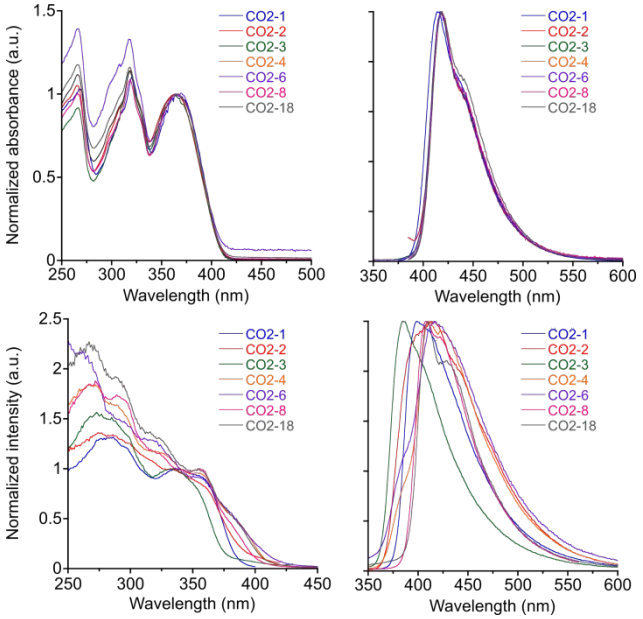

Figure 2. (Top) Absorbance and emission spectra of **CO2-R** compounds in chloroform solution (ε ~ 35000 $M^{-1}cm^{-1}$ (315 nm) in all solvents). (Bottom) Excitation and emission spectra in thermally annealed thin films, λ_{ex} = 330 nm for solution and film spectra.

3. Polymorphism

To better understand how alkyl chain length influences phase behavior, we first describe here polymorphs we have isolated of the methyl ester derivative, **CO2-1**. As described above, we previously reported single crystal X-ray structures of two polymorphs of **CO2-1**:[58] single crystals with violet emission (Em. λ_{max} = 410 nm), referred to here as **CO2-1A**, have severely twisted backbones due to cofacial stacking between ArF side chains and terminal ArH units (Figure 1).[58] Fluorescence spectra of **CO2-1** violet emitting annealed films (Em. λ_{max} = 405 nm) correspond well with those of these **CO2-1A** single crystals, suggesting the presence of this packing motif in violet emitting solids. Blue-green emitting prisms of **CO2-1** (**CO2-1B**, $\tau_F$avg = 2.2 ns) grown by slow evaporation of dichloromethane layered with hexanes (10:1 vol/vol) pack with coplanar PE backbones aggregated in slipped-stacks. These crystals (Em. λ_{max} = 465 nm) emit a spectrum similar to the blue-green fluorescent domains that often appear as minority domains in drop-cast thin films (λ_{max} = 480 nm).[58] These two polymorphs show distinct thermal properties: **CO2-1A** exhibits endothermic transitions at 139 and 173 °C, while **CO2-1B** shows a broad endotherm from 145 – 165 °C.

In addition to these forms we published previously, we have discovered two new forms of **CO2-1**: i) bluish-green emitting needles **CO2-1C** (a pseudopolymorph, *vide infra*) grown from dichloromethane/hexanes as described above for which we have solved a crystal structure bearing resemblance to **CO2-1B**, and ii) a bright green emitting powder, **CO2-1D**, grown from chloroform, for which X-ray quality single crystals

have not been obtained. The emission spectrum of **CO2-1C** ($\tau_F$avg = 1.1 ns) is nearly identical to **CO2-1B**, and exhibits a similar DSC thermogram to **CO2-1A**, with the addition of a unique endotherm at 62 °C, which we attribute to the liberation of solvent molecules (*vide infra*). Polymorph **CO2-1D**, which emerges only occasionally, emits to the red of the other polymorphs (λ_{max} = 516 nm) and displays a weak endotherm at 140 °C in the absence of other transitions.

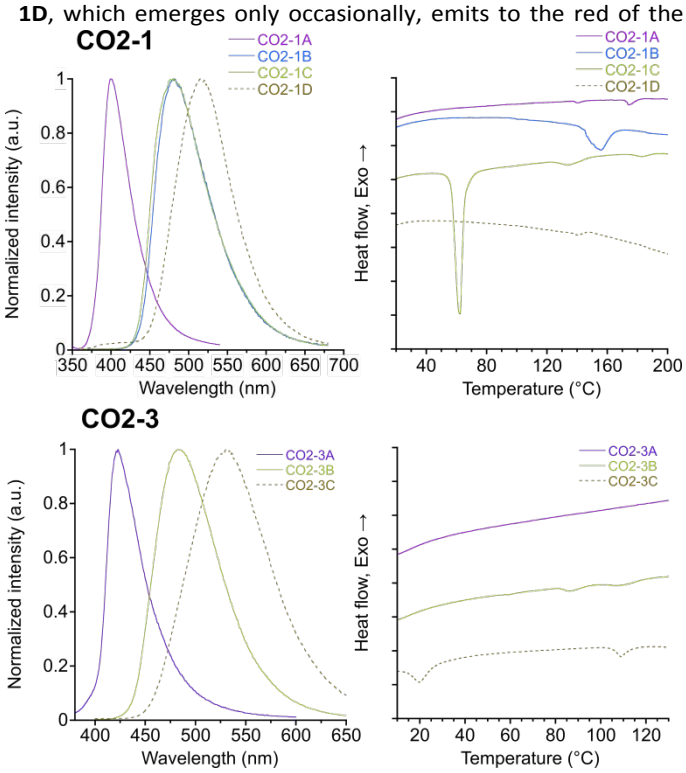

Figure 3. Emission Spectra (left) and DSC thermograms (right) for polymorphs of **CO2-1** and **CO2-3** obtained by recrystallization. Solid lines used for polymorphs whose crystal structures have been solved, and dashed lines used to indicate absence of a corresponding solved crystal structure. λ_{ex} = 330 nm.

Violet emitting crystals and powders of **CO2-1** are nearly always obtained whether solvent evaporates slowly or quickly. Blue-green emitting needles frequently appear together with the violet-emitting crystals, while bright green-emitting powder appears occasionally. Other compounds with short alkyl pendants display similar richness in solid-state phase behavior. Three polymorphs of the propyl derivative, violet emitting needles **CO2-3A** (λ_{max} = 422 nm), green emitting needles **CO2-3B** (λ_{max} = 483 nm), and bright green emitting powder **CO2-3C** (λ_{max} = 530 nm) were obtained by slow evaporation from chloroform or dichloromethane solutions. DSC thermograms of **CO2-3A** show no transitions below the melt, whereas **CO2-3B** displays two overlapping endotherms from 80 – 120 °C. **CO2-3C** shows a transition near room temperature at 20 °C, as well as an endotherm at 110 °C, similar to **CO2-3B** (Figure 3). As with **CO2-1**, crystal polymorphs **CO2-3A** and **CO2-3B** frequently occur together from slow evaporation methods, whereas powder **CO2-3C**, though reproducibly obtained by rapid evaporation of CH_2Cl_2, emerges only infrequently among the others. Lastly, we observed two polymorphs for both **CO2-2** and **CO2-4**—violet emitting crystals **CO2-2A** and **CO2-4A** (λ_{max} = 400 and 415 nm, respectively), for which we have solved crystal structures, and green emitting powders **CO2-2B** and **CO2-4B** (λ_{max} = 520 nm for both), which appear with far less frequency than the violet-emitting polymorphs, and have not yielded single crystals.

While violet and green emitting domains are frequently obtained in drop-cast films, the relative ratios of these polymorphs obtained by fast evaporation appear to depend on alkyl chain length. Spin-coated films show a mixture of bluish-green and violet emitting domains in **CO2-1**, and blue emission (mixed phases) in **CO2-2**, **CO2-3**, and **CO2-4** that gradually blue-shifts with alkyl chain length. Emission λ_{max} shifts from 474 nm in **CO2-1** to λ_{max} = 431 nm in **CO2-4** (Figure S4), which signals the increasing dominance of violet polymorphs over blue-green emitting polymorphs in mixed-phase films under these preparation conditions. Melting and slow-cooling thin films with mixed domains results in convergence to uniform violet fluorescence for all compounds regardless of the preparation method, indicating that the more hypsochromically emitting polymorphs are more stable.

With the exception of some green-emitting domains of **CO2-18** drop-cast films (Figure S3), we were unable to observe any polymorphism of molecules with longer alkyl pendants, which is similar to observations in other reports of polymorphic and responsive materials with variable lengths of alkyl pendants.[62] **CO2-**

Table 1. Photophysical data of **CO2-R** compounds in solution, drop-cast films from $CHCl_3$, and melting temperatures.

	Solution ($CHCl_3$)				Annealed Films		
PE	Abs λ_{max} (nm)	Em λ_{max} (nm)	ϕ_f	τ (ns)	Abs λ_{max} (nm)	Em λ_{max} (nm)	T_m (°C)
CO2-1	363	415	0.45	1.1	350	405	214-215
CO2-2	364	418	0.47	1.0	349	414	185-186
CO2-3	363	417	0.45	1.1	346	414	158-159
CO2-4	366	419	0.46	0.9	355	412	148-149
CO2-6	367	419	0.43	1.0	354	414	128-130
CO2-8	363	418	0.45	1.0	355	408	123-124
CO2-18	365	418	0.45	1.0	355	410	112

This journal is © The Royal Society of Chemistry 20xx

Please do not adjust margins

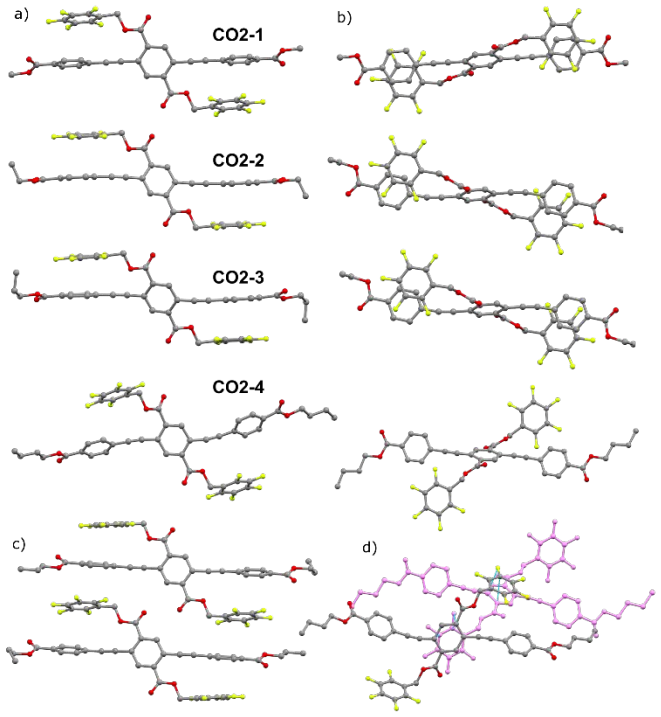

Figure 4. a) Structures from violet emitting crystals of **CO2-1** - **CO2-4** showing twisted PEs. b) View of PEs along face of ArF ring, showing lateral displacements with respect to PE main chain. c) Intramolecular and intermolecular ArF-ArH stacking in CO2-3. d) Only intermolecular ArF-ArH stacking observed in CO2-4. Second PE highlighted magenta for clarity, with short contacts in ArF-ArH displayed. Hydrogens omitted for clarity.

6, **CO2-8**, and **CO2-18** yielded only colorless powders with violet fluorescence regardless of preparation conditions. We attribute the prevalence of polymorphism throughout the compounds with shorter alkyl chains to "soft" non-covalent control: spectroscopic results indicate that although ArF-ArH interactions with moderately electron-withdrawing alkyl esters (σ_p = 0.45 for $-CO_2Me$)[63] are strong enough to cause the twisted, non-aggregated packing motifs to be thermodynamically favorable, such interactions are sufficiently weak to accommodate alternative arrangements, such as coplanar, aggregated PE backbones yielding blue-green fluorescence. The relative absence of polymorphism in **CO2-6**, **CO2-8**, and **CO2-18** suggests that interactions of alkyl chains shifts this delicate balance to favor programmed twisting more thoroughly.

4. Structures of Violet Emitting Crystals

Single crystal X-ray structures of fluorescent prisms and needles of **CO2-2A**, **CO2-3A**, and **CO2-4A**, grown by slow evaporation from ethyl acetate, acetone, and chloroform, support the assignment of violet-emitting polymorphs to twisted PEs that resist aggregation. Similar to the methyl ester derivative (*vide supra*), structures of **CO2-2A** and **CO2-3A** feature twisted backbones (69-76 and 67-77° torsional angles, respectively), as well as coplanar interactions between side chain perfluorinated arenes and the terminal benzoate rings of the conjugated PE backbone (3.9-4.1 Å ArF-ArH centroid-centroid distances). In these structures, intermolecular ArF-ArH stacking extends above and below the PEs, yielding infinite columns of twisted units, which pack with each other in herringbone-like structures. Adjacent columns of stacked PEs are diagonally offset from one another across the molecular long axis (Figure S5), accommodating edge-face interactions between terminal benzoates and terephthalates (3.3 – 3.5 Å closest contacts), as well as between pendant perfluoroarenes and terephthalates (3.0 – 3.1 Å closest contacts).[58] The ArF-ArH interactions in **CO2-2A** and **CO2-3A** are slightly elongated relative to **CO2-1A** (3.8 Å ArF-ArH centroid-centroid distance). Ethyl and propyl side chains are further displaced laterally with respect to the PE backbones (Figure 4b) as the ArF pendants extend at ~18° angles away from the plane of the central terephthalate, rather than the 8° offset in **CO2-1A**. These minor differences aside, the ethyl or propyl chains of these derivatives yield only small changes in crystal packing relative to **CO2-1A**, and otherwise lead to increased unit cell volume per PE and decreased calculated density with respect to **CO2-1A** (Table S2).

The butyl chains of **CO2-4A**, however, change crystal packing more notably compared to those with shorter alkyl chains. The PE backbone is less twisted (43–61°), and intramolecular ArF-ArH stacking is absent (6.1-6.2Å centroid-centroid distances). The butyl chains of adjacent molecules occupy the regions of space that contain ArF rings in the other twisted structures, which blocks intramolecular ArF-ArH stacking (Figure S6). Rather than the vertical, columnar stacking of twisted PEs when intramolecular ArF-ArH stacking

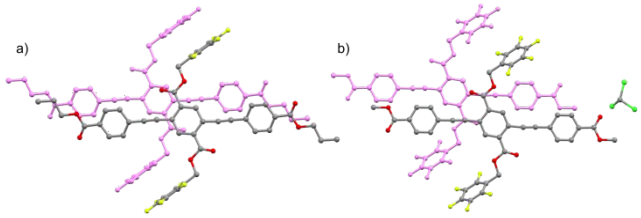

Figure 5. Structures of blue-green emitting crystals showing coplanar PE backbones and aggregated packing of PEs in a) **CO2-3B** and b) **CO2-1C**, which includes a $CHCl_3$ molecule. Hydrogens omitted for clarity, and aggregated PEs highlighted magenta.

occurs, the strictly intermolecular ArF-ArH interactions of **CO2-4A** yield networks of diagonally stacked PEs (Figures S5 and S6). Therefore, although they do not strongly impact the optical properties of the violet emitting phases, the lengths of alkyl chains do influence the mode of crystal packing. Based on their optical properties, we therefore suspect that solids **CO2-**

This journal is © The Royal Society of Chemistry 20xx

Please do not adjust margins

6, **CO2-8**, and **CO2-18** lack intramolecular stacking between PEs and side chains, while still having twisted structures and intermolecular ArF-ArH interactions throughout.

5. Structures and Crystal-to-Crystal Transitions of Blue-Green Emitting Polymorphs

To better understand the impact of packing on the different optical properties of polymorphs, we determined single crystal X-ray structures of additional blue-green emitting polymorphs of **CO2-1** and **CO2-3**. Each of these crystal structures exhibit generally coplanar PE rings and slipped-stacked pendants that do not interact with PE main chains. A needle of **CO2-3B** grown by slow evaporation of dichloromethane/hexanes (10:1 vol/vol) shows PEs with 21° torsional angles aggregated in infinite slipped stacks (3.4 Å closest contacts), similar to the coplanar structure **CO2-1B** (Figure 1, τ_F (avg) = 2.2 ns). Alternating columns of aggregated PEs in **CO2-3B** are nearly perpendicular to one another with close contacts between carbonyls and and neighboring carbon atoms in perfluoroarenes (2.9 Å C=O---C-F distances). In addition, pseudopolymorph **CO2-1C** grown by the same method shows a nearly identical structure to **CO2-1B,**[58] but includes one chloroform molecule per unit cell (Figure 5), which likely accounts for the endothermic transition at 62 °C (Figure 3).

TD-DFT calculations on individual molecules from these crystal structures support the importance of conformation in their optical properties (Figure S7). Comparing the experimental excitation spectra of **CO2-1A** and **CO2-1B** single crystals reveals a 50 nm red-shift in the spectrum shoulder (λ = 375 and 425 nm, respectively). Likewise, simulated UV-Vis spectra from TD-DFT calculations (B3LYP/6-31G(d,p)) exhibit a 53 nm red-shift in the absorbance λ_{max} between these twisted and planar structures (339 and 392 nm, respectively). Similar results are observed for the **CO2-3** polymorphs. Excitation spectra show a 45 nm red-shift between single crystals of **CO2-3A** and **CO2-3B** (λ = 380 and 425 nm, respectively), and their corresponding simulated UV-Vis spectra exhibit a 66 nm red-shift in absorbance λ_{max} (334 and 400 nm, respectively) as a result of increased conjugation in the planarized structure.

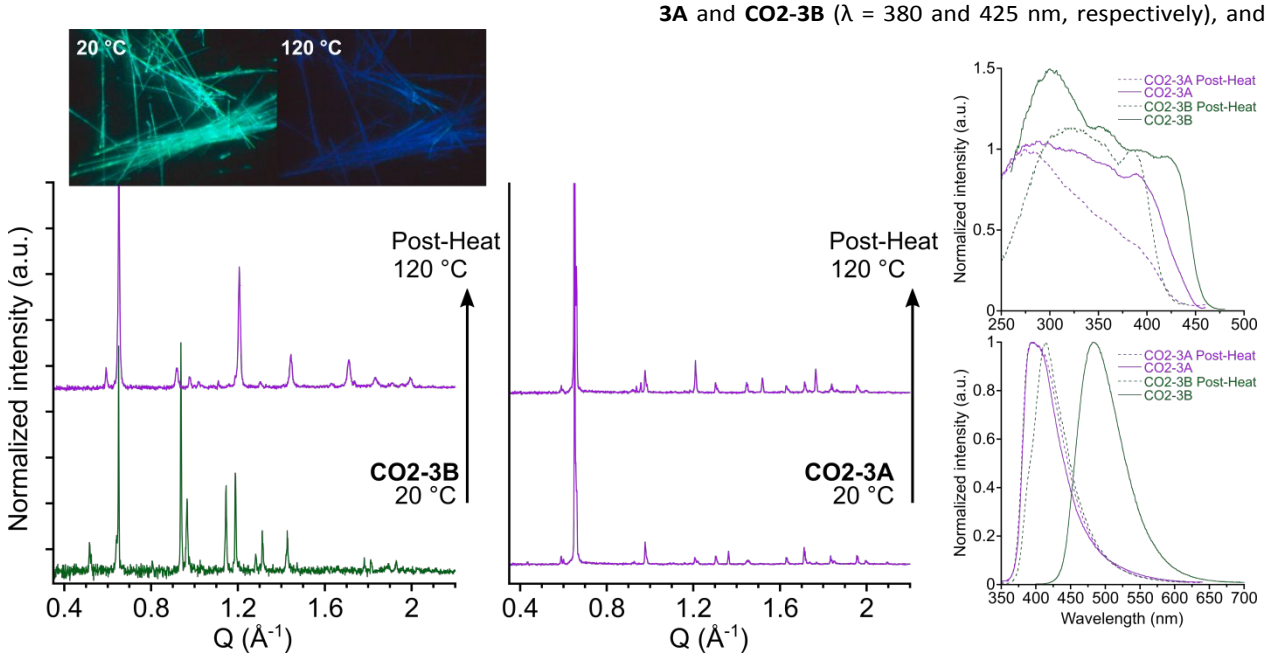

Figure 6. Thermal transition of **CO2-3B**. (Left) PXRD (λ = 1.54184 Å) shows patterns of green and violet emitting polymorphs at room temperature and after heating to 120 °C, with accompanying photos of green emissive **CO2-3B** before and after heating. Corresponding excitation and emission spectra (top and bottom right, respectively) of the polymorphs before and after heating indicate transformation to violet fluorescence after heating. λ_{ex} = 330 nm.

Emitting Polymorphs

In addition, blue-green emitting crystals **CO2-1B** (Figure S8) and **CO2-3B** (Figure 6) undergo transitions to crystalline violet-emitting polymorphs upon heating, while preserving crystal habit. Corresponding with the broad transition seen in DSC (Figure 3), violet emitting domains appear within prisms of **CO2-1B** (roughly 2 x 0.2 x 0.2 mm) at 150 °C and propagate along the length of the crystals, suggesting a nucleation-and-growth type mechanism of the phase transition.[10] Emission spectra of these crystals after heating (λ_{max} = 413 nm) are nearly identical to those when polymorph **CO2-1A** is also heated to 200 °C, including shoulders in excitation spectra at 375 nm. The green-emitting polymorph **CO2-3B** of the propyl ester behaves similarly: green emitting needles bend and twist between 80 – 120 °C while their fluorescence becomes violet (λ_{max} = 413 nm).

Although we were unable to solve the unit cells of heated crystals, powder X-ray diffraction (PXRD) confirms the structural transformations. Diffractograms of **CO2-1A** and **CO2-1B** at room temperature show different patterns that become more similar after heating (Figure S8). In agreement with the DSC data, PXRD analysis of the **CO2-3B** also confirms a thermal transition between polymorphs upon heating to 120 °C (Figure S6). Based on the spectroscopic changes, we conclude that the samples after heating have twisted, non-aggregated packing

This journal is © The Royal Society of Chemistry 20xx

Please do not adjust margins

motifs based on the fluorescence spectra being similar to solved twisted structures.

Given the similarity in crystal packing between the **CO2-1B** and **CO2-3B** structures, we conclude that the longer alkyl chains of the propyl derivative facilitating these thermal transitions at lower temperatures, such as by stabilizing the twisted structures of the A phases relative to the planar, aggregated structures of the B phases. Alkyl pendants can modulate thermally induced phase transitions via changes in the mode of crystal packing,[64] changes in lattice energies of stable vs metastable phases,[56,65,66] or changes in the balance of phase enthalpy and entropy.[67] Furthermore, given the similarities in crystal density between the twisted and planar forms (CO2-1B: 1.513 and CO2-1A: 1.583 g/cm^3, CO2-3B: 1.556 and CO2-3A: 1.522 g/cm^3) the changes in crystal stability are likely due to alkyl chains tipping the balance of non-covalent interactions to favor the twisted phases over the coplanar, aggregated phase, rather than close packing considerations.

Similar hypsochromically-shifting polymorphic transitions occur for polymorphs **CO2-1C** and **CO2-1D** from 150 – 200 °C, as well as in **CO2-2B** powder from 60 – 130 °C, which agrees with the endotherm observed at 56 °C (Figure S2). Only **CO2-4B** powder, which shows no thermal transitions below its melting point by DSC, does not change from green fluorescence upon heating, even though melting followed by slow-cooling gives uniform violet emission. Despite these thermally induced polymorphic transitions among **CO2-1** to **CO2-4**, blue and green emitting phases are generally unresponsive to solvent vapor fuming, showing unchanged fluorescence after exposure to CH_2Cl_2 vapor. In all cases, however, melting and slow-cooling of any of these polymorphs for **CO2-1** to **CO2-4** results in convergence on violet emitting phases, suggesting that twisted arrangements of PEs with some form of ArF-ArH directed packing resulting in violet emission give stable phases, whereas the blue and green emitting phases with coplanar/aggregated PEs are metastable.

6. Reversible Mechanofluorochromism of Powders and Films

In conjunction with these accessible polymorphs, this family of **CO2-R** compounds exhibits reversible MFC upon mechanical grinding of powders and films, resulting in consistent bathochromic shifts from violet to green emission with $\Delta\lambda_{max}$ of emission of 36 – 80 nm (Table S3). The responses of these sheared films reverse fully upon heating below their melting temperatures or fuming with CH_2Cl_2 solvent vapor, and repeating this reversible process for **CO2-1** over multiple cycles does not fatigue the MFC response (Figure S10). In conjunction with the crystal structures of blue-green emitting polymorphs, we attribute this MFC to increased backbone planarization and/or aggregation of initially twisted structures.[59,68] Thermograms obtained from DSC of **CO2-1** after grinding exhibits an irreversible exothermic peak from 40 – 50 °C in the first heat, suggesting a crystalline-to-amorphous transition with grinding and cold-crystallization during thermal recovery (Figure S11). However, thermograms of other **CO2-R** ground powders did not show any differences from recrystallized powders, which suggests small differences in energy between the ground and annealed phases.

While there is little difference in the green fluorescence obtained by grinding any of the **CO2-R** compounds, temperatures required for thermal recovery depend strongly on alkyl chain length, ranging from room temperature for **CO2-4**, **CO2-6**, and **CO2-8** to 100 °C for **CO2-1**. For example, recovery of emission to λ_{max}

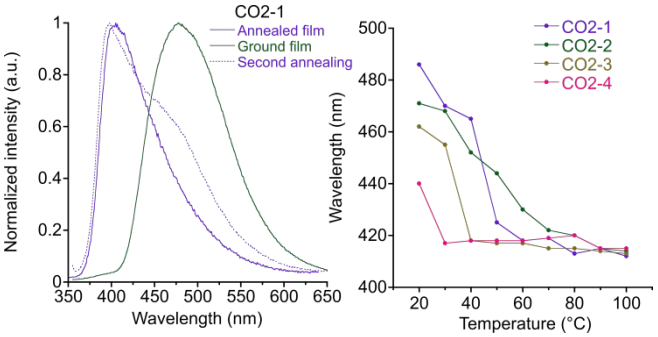

Figure 7. Mechanofluorochromism in **CO2-R** films. (Left) Representative MFC response in emission spectra of **CO2-1**, grinding with a spatula and thermally annealing at 180 °C. (Right) Plot of emission maxima of ground films while heating at 10 °C increments to 100 °C demonstrating how compounds with longer alkyl chain recover violet fluorescence across lower temperatures. See corresponding images and spectra, Fig S10. λ_{ec} = 330 nm.

~415 nm occurs at 30 °C for **CO2-4** and remains unchanged for increasing temperatures thereafter, whereas **CO2-3**, **CO2-2**, and **CO2-1** show a gradient in their recovered emission with λ_{max} = 455, 468, and 470 nm, respectively, at 30 °C (Figure 8 and corresponding Figure S12). At 40 °C, **CO2-3** shows near complete recovery to λ_{max} = 418 nm, while **CO2-2** and **CO2-1** require higher temperatures and recover gradually up until 90 °C, changing only slightly at even higher temperatures.

With alkyl chains longer than propyl, recovery of violet emission occurs at room temperature. Upon grinding **CO2-4**, bright green fluorescence dissipates within seconds, after which a less intense emission spectrum with λ_{max} = 440 nm hypsochromically shifts to 418 nm within 2 minutes (Figure S13). **CO2-6** and **CO2-8** recover their violet emission on the order of one second at room temperature, allowing for mechanical "writing" into the waxy films that disappears rapidly (Video S2). Films of **CO2-18** notably break from this trend, exhibiting persistent green emission at room temperature after shearing (Em. λ_{max} = 472 nm, $\Delta\lambda_{max}$ = 62 nm) and requiring thermal annealing to 80 °C to recover (Figure S14). Given the greater rigidity and crystallinity of **CO2-18** powders relative to **CO2-8** and **CO2-6**, we conclude that the extensive dispersion interactions of alkyl chains alters solid packing and phase stability to change the nature of solid phase transitions in **CO2-18**. Among these compounds, increasing alkyl chain length may decrease temperatures required to recover violet emission after grinding by lowering the kinetic barrier to transition from metastable coplanar/aggregated assemblies to crystalline, twisted assemblies. This general trend of decreasing MFC thermal recovery temperatures with alkyl chain length is consistent with our observations on the overall occurrence of polymorphism in these compounds and decreasing temperatures in thermal polymorphic transitions that converge on violet emitting phases with alkyl chain length.

This journal is © The Royal Society of Chemistry 20xx

Conclusions

This series of seven ester-terminated PEs with relatively weak ArF-ArH interactions show alkyl chain length dependent polymorphism related both to irreversible thermochromic green-to-violet fluorescent crystal-to-crystal transitions, as well as reversible violet-to-green mechanofluorochromism. Shorter chain lengths lead to greater co-incidence of green emitting polymorphs (planar/aggregated) with the violet emitting phase (programmed twisting), while longer chain lengths preferentially stabilize the violet emitting phase, leading both to lower temperatures of crystal-to-crystal transitions and lower thermal recovery temperatures in the MFC process. Crystallography reveals how these trends relate to the changes in PE packing and interactions with chain length; as alkyl chains modulate the intramolecular vs intermolecular nature of the ArF-ArH programmed twisting, conformational distortions of the twisted motif determine its relative stability and ease of transition from planar/aggregated to the twisted structures.

The structure-tunable polymorphism in these PEs demonstrates how the balance of competing interactions and packing forces can be leveraged to obtain and control stimuli-responsive behavior in molecular assemblies, most importantly by employing a modular non-covalent control unit in non-conjugated side chains. Questions remain as to how these principles will extend beyond small molecules, such as in polymers, and the discovery of additional polymorphs of all compounds is always possible. Nevertheless, we suggest that directed but purposefully weak interactions enable access to polymorphs and interconversion between them, particularly in torsionally flexible molecules. In such cases, small structural modifications that alter competition between interactions can tune the access to and interconversion between polymorphs in a rational way, thereby addressing a major roadblock for translating new conjugated materials into functional devices.

Conflicts of interest

The authors declare no conflicts of interest.

Acknowledgements

The authors thank the U.S. Department of Energy, Basic Energy Sciences (DE-SC0016423), for generous support of this research. The authors would like to acknowledge the beamtime of 16D-LiX at the NSLS-II (Brookhaven National Lab) through a beamtime proposal (BAG-302208). The LiX beamline is part of the Life Science Biomedical Technology Research resource, jointly supported by the National Institute of Health, National Institute of General Medical Sciences under Grant P41 GM111244, and by the Department of Energy Office of Biological and Environmental Research under Grant KP1605010, with additional support from NIH Grant S10 OD012331. NSLS-II is a U.S. Department of Energy (DOE) Office of Science User Facility operated for the DOE Office of Science by Brookhaven National Laboratory under Contract No. DE-SC0012704. The authors would like to thank Dr. Lin Yang, who manages the Life Science X-ray Scattering (LiX) at Brookhaven National Laboratory for support with WAXS measurements and Dr. Daniela Morales, X-Ray Diffraction Lab at University of Connecticut Institute of Materials Science for support with PXRD measurements.

Notes and references

1 Z. B. Henson, K. Müllen and G. C. Bazan, *Nat. Chem.*, 2012, **4**, 699–704.
2 C. Sutton, C. Risko and J.-L. Brédas, *Chem. Mater.*, 2016, **28**, 3–16.
3 A. Pulido, L. Chen, T. Kaczorowski, D. Holden, M. A. Little, S. Y. Chong, B. J. Slater, D. P. McMahon, B. Bonillo, C. J. Stackhouse, A. Stephenson, C. M. Kane, R. Clowes, T. Hasell, A. I. Cooper and G. M. Day, *Nature*, 2017, **543**, 657–664.
4 C. Botta, S. Benedini, L. Carlucci, A. Forni, D. Marinotto, A. Nitti, D. Pasini, S. Righetto and E. Cariati, *J. Mater. Chem. C*, 2016, **4**, 2979–2989.
5 J. Yang, Z. Ren, B. Chen, M. Fang, Z. Zhao, B. Z. Tang, Q. Peng and Z. Li, *J. Mater. Chem. C*, 2017, **5**, 9242–9246.
6 G. Zhang, J. Lu, M. Sabat and C. L. Fraser, *J. Am. Chem. Soc.*, 2010, **132**, 2160–2162.
7 G. R. Desiraju, *Angew. Chemie - Int. Ed.*, 2007, **46**, 8342–8356.
8 Q. Kong, W. Zhuang, G. Li, Y. Xu, Q. Jiang and Y. Wang, *New J. Chem.*, 2017, **41**, 13784–13791.
9 K. Wang, H. Zhang, S. Chen, G. Yang, J. Zhang, W. Tian, Z. Su and Y. Wang, *Adv. Mater.*, 2014, **26**, 6168–6173.
10 J. D. Dunitz, *Pure Appl. Chem.*, 1991, **63**, 177–185.
11 A. J. Cruz-Cabeza, S. M. Reutzel-Edens and J. Bernstein, *Chem. Soc. Rev.*, 2015, **44**, 8619–8635.
12 P. M. Piaggi and M. Parrinello, *Proc. Natl. Acad. Sci.*, 2018, **115**, 10251–10256.
13 R. Dubey, M. S. Pavan and G. R. Desiraju, *Chem. Commun.*, 2012, **48**, 9020–9022.
14 F. Musil, S. De, J. Yang, J. E. Campbell, G. M. Day and M. Ceriotti, *Chem. Sci.*, 2017, 1289–1300.
15 S. Varughese, *J. Mater. Chem. C*, 2014, **2**, 3499–3516.
16 G. R. Desiraju, *J. Am. Chem. Soc.*, 2013, **135**, 9952–9967.
17 G. E. Purdum, N. G. Telesz, K. Jarolimek, S. M. Ryno, T. Gessner, N. C. Davy, A. J. Petty, Y. Zhen, Y. Shu, A. Facchetti, G. E. Collis, W. Hu, C. Wu, J. E. Anthony, R. T. Weitz, C. Risko and Y. L. Loo, *J. Am. Chem. Soc.*, 2018, **140**, 7519–7525.
18 D. R. Islamov, V. G. Shtyrlin, N. Y. Serov, I. V. Fedyanin and K. A. Lyssenko, *Cryst. Growth Des.*, 2017, **17**, 4703–4709.
19 M. Jin, T. Seki and H. Ito, *J. Am. Chem. Soc.*, 2017, **139**, 7452–7455.
20 F. C. Pigge, *CrystEngComm*, 2011, **13**, 1733.
21 D. Yan and D. G. Evans, *Mater. Horizons*, 2014, **1**, 46.
22 C. P. Brock, W. B. Schweizer and J. D. Dunitz, *J. Am. Chem. Soc.*, 1991, **113**, 9811–9820.
23 J. Mei, N. L. C. Leung, R. T. K. Kwok, J. W. Y. Lam and B. Z. Tang, *Chem. Rev.*, 2015, **115**, 11718–11940.
24 Z. Zhuang, P. Shen, S. Ding, W. Luo, B. He, H. Nie, B. Wang, T. Huang, R. Hu, A. Qin, Z. Zhao and B. Z. Tang, *Chem. Commun.*, 2016, **52**, 10842–10845.
25 Z. Chen, G. Liu, S. Pu and S. Hua, 2017, **143**, 409–415.

This journal is © The Royal Society of Chemistry 20xx

Please do not adjust margins

26 P. S. Hariharan, G. Parthasarathy, A. Kundu, S. Karthikeyan, Y. Sagara, D. Moon and S. P. Anthony, *Cryst. Growth Des.*, 2018, **18**, 3971–3979.

27 R. Li, S. Xiao, Y. Li, Q. Lin, R. Zhang, J. Zhao, C. Yang, K. Zou, D. Li and T. Yi, *Chem. Sci.*, 2014, **5**, 3922.

28 Z. He, L. Zhang, J. Mei, T. Zhang, J. W. Y. Lam, Z. Shuai, Y. Q. Dong and B. Z. Tang, *Chem. Mater.*, 2015, **27**, 6601–6607.

29 A. Mukherjee, *Cryst. Growth Des.*, 2015, **15**, 3076–3085.

30 L.-Z. W. Zhanting Li, D.-W. Zhang, H. Wong and Z. Ting-Li, *Hydrogen Bonded Supramolecular Structures*, Springer-Verlag, Berlin, 2015.

31 G. Berger, J. Soubhye and F. Meyer, *Polym. Chem.*, 2015, **6**, 3559–3580.

32 K. Kishikawa, *Isr. J. Chem.*, 2012, **52**, 800–808.

33 S. Roy, A. Hazra, A. Bandyopadhyay, D. Raut, P. L. Madhuri, D. S. S. Rao, U. Ramamurty, S. K. Pati, S. Krishna Prasad and T. K. Maji, *J. Phys. Chem. Lett.*, 2016, 4086–4092.

34 L. Yu, *Acc. Chem. Res.*, 2010, **43**, 1257–1266.

35 J. Wu, Y. Cheng, J. Lan, D. Wu, S. Qian, L. Yan, Z. He, X. Li, K. Wang, B. Zou and J. You, *J. Am. Chem. Soc.*, 2016, **138**, 12803–12812.

36 Y. Sagara, T. Mutai, I. Yoshikawa and K. Araki, *J. Am. Chem. Soc.*, 2007, **129**, 1520–1521.

37 X. Du, F. Xu, M. Sen Yuan, P. Xue, L. Zhao, D. E. Wang, W. Wang, Q. Tu, S. W. Chen and J. Wang, *J. Mater. Chem. C*, 2016, **4**, 8724–8730.

38 J. Guan, F. Xu, C. Tian, L. Pu, M. Yuan and J. Wang, 2019, 216–222.

39 M. Sen Yuan, D. E. Wang, P. Xue, W. Wang, J. C. Wang, Q. Tu, Z. Liu, Y. Liu, Y. Zhang and J. Wang, *Chem. Mater.*, 2014, **26**, 2467–2477.

40 W. A. Morris, M. Sabat, T. Butler, C. A. Derosa and C. L. Fraser, *J. Phys. Chem. C*, 2016, **120**, 14289–14300.

41 X. Huang, L. Qian, Y. Zhou, M. Liu, Y. Cheng and H. Wu, *J. Mater. Chem. C*, 2018, **6**, 5075–5096.

42 Q. Kong, W. Zhuang, G. Li, Y. Xu, Q. Jiang and Y. Wang, *New J. Chem.*, 2017, **41**, 13784–13791.

43 C. Ge, J. Liu, X. Ye, Q. Han, L. Zhang, S. Cui, Q. Guo, G. Liu, Y. Liu and X. Tao, *J. Phys. Chem. C*, 2018, **122**, 15744–15752.

44 T. Seki and H. Ito, *Chem. - A Eur. J.*, 2016, 4322–4329.

45 Y. Sagara, S. Yamane, M. Mitani, C. Weder and T. Kato, *Adv. Mater.*, 2016, **28**, 1073–1095.

46 Y. Zhou, Y. Liu, Y. Guo, M. Liu, J. Chen, X. Huang, W. Gao, J. Ding, Y. Cheng and H. Wu, *Dye. Pigment.*, 2017, **141**, 428–440.

47 T. Butler, F. Wang, M. Sabat and C. L. Fraser, *Mater. Chem. Front.*, 2017, **1**, 1804–1817.

48 G. R. Krishna, R. Devarapalli, R. Prusty, T. Liu, C. L. Fraser, U. Ramamurty and C. M. Reddy, *IUCrJ*, 2015, **2**, 611–619.

49 Y. Zhang, G. Zhuang, M. Ouyang, B. Hu, Q. Song, J. Sun, C. Zhang, C. Gu, Y. Xu and Y. Ma, *Dye. Pigment.*, 2013, **98**, 486–492.

50 L. Bu, M. Sun, D. Zhang, W. Liu, Y. Wang, M. Zheng, S. Xue and W. Yang, *J. Mater. Chem. C*, 2013, **1**, 2028–2035.

51 S. Xue, X. Qiu, Q. Sun and W. Yang, *J. Mater. Chem. C*, 2016, **4**, 1568–1578.

52 N. D. Nguyen, G. Zhang, J. Lu, A. E. Sherman and C. L. Fraser, *J. Mater. Chem.*, 2011, **21**, 8409.

53 Q. K. Sun, W. Liu, S. A. Ying, L. L. Wang, S. F. Xue and W. J. Yang, *RSC Adv.*, 2015, **5**, 73046–73050.

54 Y. Xiong, Y. Ma, X. Yan, G. Yin and L. Chen, *RSC Adv.*, 2015, **5**, 53255–53258.

55 M. Zheng, D. T. Zhang, M. X. Sun, Y. P. Li, T. L. Liu, S. F. Xue and W. J. Yang, *J. Mater. Chem. C*, 2014, **2**, 1913–1920.

56 Y. Wang, W. Liu, L. Bu, J. Li, M. Zheng, D. Zhang, M. Sun, Y. Tao, S. Xue and W. Yang, *J. Mater. Chem. C*, 2013, **1**, 856–862.

57 R. H. Pawle, T. E. Haas, P. Müller and S. W. Thomas, *Chem. Sci.*, 2014, **5**, 4184–4188.

58 S. A. Sharber, R. N. Baral, F. Frausto, T. E. Haas, P. Müller and S. W. Thomas, *J. Am. Chem. Soc.*, 2017, **139**, 5164–5174.

59 S. A. Sharber, K. C. Shih, A. Mann, F. Frausto, T. E. Haas, M. P. Nieh and S. W. Thomas, *Chem. Sci.*, 2018, **9**, 5415–5426.

60 C. J. Lin, S. K. Kundu, C. K. Lin and J. S. Yang, *Chem. - A Eur. J.*, 2014, **20**, 14826–14833.

61 R. H. Pawle, V. Eastman and S. W. Thomas, *J. Mater. Chem.*, 2011, **21**, 14041–14047.

62 Y. Lei, Y. Zhou, L. Qian, Y. Wang, M. Liu, X. Huang, G. Wu, H. Wu, J. Ding and Y. Cheng, *J. Mater. Chem. C*, 2017, **5**, 5183–5192.

63 C. Hansch, a Leo and R. W. Taft, *Chem. Rev.*, 1991, **91**, 165–195.

64 P. S. Hariharan, P. Gayathri, D. Moon and S. P. Anthony, *ChemistrySelect*, 2017, **2**, 7799–7807.

65 G. G. Shan, H. Bin Li, H. T. Cao, H. Z. Sun, D. X. Zhu and Z. M. Su, *Dye. Pigment.*, 2013, **99**, 1082–1090.

66 X. Zhang, Z. Chi, B. Xu, L. Jiang, X. Zhou, Y. Zhang, S. Liu and J. Xu, *Chem. Commun.*, 2012, **48**, 10895.

67 Z. Q. Yu, J. W. Y. Lam, C. Z. Zhu, E. Q. Chen and B. Z. Tang, *Macromolecules*, 2013, **46**, 588–596.

68 S. A. Sharber and S. W. Thomas, *Chem. - A Eur. J.*, 2018, **24**, 16987–16991.

This journal is © The Royal Society of Chemistry 20xx

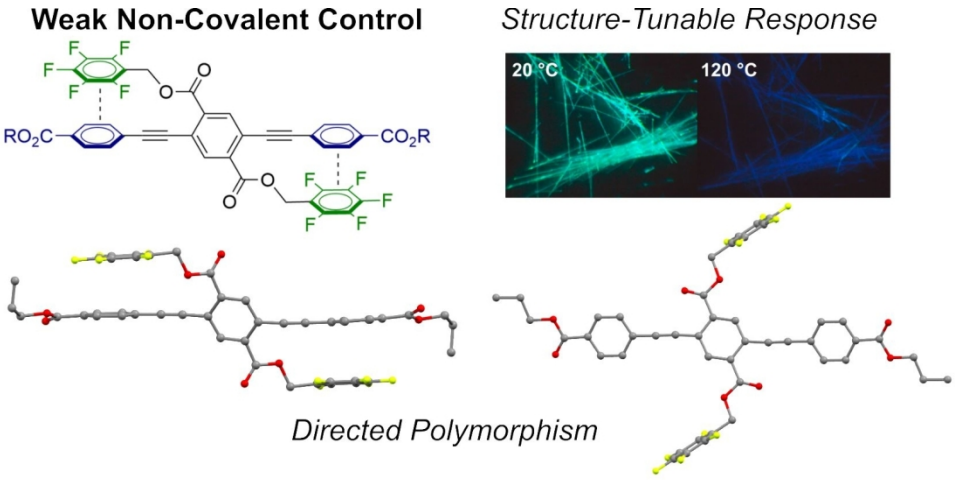

458x218mm (96 x 96 DPI)